RSC Advances

PAPER

View Article Online
View Journal | View Issue

Cite this: *RSC Adv.*, 2015, **5**, 104829

Corrosion and tribocorrosion performance of multilayer diamond-like carbon film in NaCl solution

Mingjun Cui,[ac] Jibin Pu,[b] Jun Liang,[a] Liping Wang,*[ab] Guangan Zhang*[a] and Qunji Xue[a]

The anticorrosion and tribocorrosion properties of a multilayer diamond-like carbon (DLC) film were systematically investigated in NaCl solution. Electrochemical measurements suggest that the corrosion performance of the multilayer DLC film is superior to those of the substrate and single layer DLC film in NaCl solution, which is attributed to the successively multilayered structure with a well-bonded interface and the formation of Si oxides. An extremely high Warburg impedance value, higher than 10^7 Ω cm^2, of the multilayer DLC film has been observed. Tribocorrosion tests show that the multilayer DLC film presents lower wear rate in NaCl solution, with the substrate and single layer DLC film as comparisons. We demonstrate that the multilayer DLC film is an excellent protective material for improving both corrosion and wear performance of the substrate.

Received 13th October 2015
Accepted 30th November 2015

DOI: 10.1039/c5ra21207c

www.rsc.org/advances

1. Introduction

Some stainless steel components are subjected to simultaneous wear and corrosion in corrosive environments, which leads to accelerated degradation of the components, such as in offshore, mining, power generation, biomedical and food processing applications.[1–3] Therefore, it is very significant to take some protective measures to improve corrosion performance of the substrate, thereby extending the lifetime of these components. Although a lot of work has reported that coatings such as TiN, CrN and polymers could improve the corrosion resistance of the substrates, the impedance values of these coatings (10^4–10^6 Ω cm^2) were lower than those of DLC films (10^5–10^8 Ω cm^2).[4–7] Consequently, we consider that the DLC film is a promising candidate for corrosion protection for metals due to its high hardness, chemical inertness and tribological properties.[8–10]

However, as protective coatings, the high intrinsic stresses and through-film thickness defects associated with films' deposition give rise to poor adhesion strength and corrosion resistance.[11,12] Functional grading,[4] doping[12–16] and multilayer structure[17] with interlayer have been widely used to overcome these problems. Particularly, the intrinsic stress can be effectively reduced by designing multilayer systems.[17–19] Moreover, the successively multilayer structure can neutralize defects, like pores, crevices or columnar structure occurring in the single layer DLC films so that the ion transportation path is prolonged or blocked.[4,5,17,20–22] Whereas, there is rarely work on the corrosion performance of the multilayer DLC films in corrosive medium. Wang *et al.* has reported that the multilayer DLC film can effectively prevent the substrate from long-term corrosion attack due to the minimization of sub micro-scale defects by corrosion product deposition.[17] Nonetheless, the impedance value of the multilayer DLC film reported decreased dramatically after long-term corrosion attack.

In our previous work, super thick Si doped multilayer DLC film that was composed of two different alternative materials had been successfully deposited on steel substrate by plasma enhanced chemical vapor deposition (PECVD) method, exhibiting excellent mechanical and tribological properties.[18,23] Consequently, in the present study, Si doped multilayer DLC film was prepared by PECVD method. Its corrosion resistance was evaluated through electrochemical measurements in NaCl solution, with the thin single layer DLC film and substrate as a comparison. Finally, tribocorrosion properties of the multilayer DLC film were preliminary investigated.

2. Experimental details

2.1 Preparation of the DLC films

The multilayer DLC film was deposited on the steel substrate and Si substrate using PECVD method. Firstly, the substrates were cleaned ultrasonically in acetone and ethanol for 20 min, respectively. Then the substrates were etched in Ar plasma for

[a]*State Key Laboratory of Solid Lubrication, Lanzhou Institute of Chemical Physics, Chinese Academy of Sciences, Lanzhou 730000, China. E-mail: lpwang@licp.cas.cn; gazhang@licp.cas.cn; Fax: +86 931 4968163; Tel: +86 931 4968080*

[b]*Key Laboratory of Marine Materials and Related Technologies, Ningbo Institute of Materials Technology and Engineering, Chinese Academy of Sciences, Ningbo 315201, China*

[c]*University of Chinese Academy of Sciences, Beijing 100039, China*

30 min at a bias of −5 kV in order to remove the surface contaminants. The Si transition layer was obtained at a bias voltage of −15 kV and pressure of 15 Pa by introducing silane (SiH_4) into the vacuum chamber for 15 min in order to improve adhesion to substrate. Then, the multilayer DLC film (Si_x-DLC/Si_y-DLC)$_n$ consisting of alternating Si_x-DLC (low-Si-doped DLC layer) and Si_y-DLC (high-Si-doped DLC layer) layers was deposited at a bias voltage of −0.8 kV by introducing a mixture of acetylene (C_2H_2) and silane (SiH_4), n is the number of (Si_x-DLC/Si_y-DLC) layers ($n = 10$). Finally, a DLC top layer was deposited for 20 min as surface layer. The multilayer structure was aimed at reducing the intrinsic stress and the possibility of pinholes growing throughout the entire film. The formation of Si–C bond in DLC films can also relieve stress in a longer-range order due to the difference in the bond lengths between Si–C (1.89 Å) and C–C (1.54 Å).[18,24] In addition, the single layer DLC film was prepared by PECVD method for comparison. The cleaning process and the deposition of Si transition layer were same with the preparation of multilayer DLC film. And the single layer DLC film was deposited at a bias voltage of −0.8 kV with acetylene (C_2H_2) as precursor. The detailed parameters were listed in Table 1.

2.2 General characterization

The cross-sectional structure, morphology and surface roughness of the DLC films were measured with field emission scanning electron microscopy (FESEM, S-4800, HITACHI) and atomic force microscopy (AFM, CSPM4000, Benyuan, China). Energy dispersive spectroscopy (EDS) and Auger electron spectroscopy (AES, PHI-700, ULVAC) were used to obtain the chemical depth profile of the films. Crystal structure of the samples was assessed by high-resolution transmission electron microscopy (HRTEM, JEM-1200EX) and X-ray diffraction (XRD, XPERT-PRO) using Cu-Kα radiation from 20° to 80°, respectively. The chemical states of the elements were analyzed by X-ray photoelectron spectroscope (XPS, PHI-5702) using K-alpha irradiation as the excitation source. The binding energies of the target elements were determined at a pass energy of 29.3 eV, using the binding energy of contaminated carbon (C 1s: 284.8 eV) as the reference. A scratch tester (MFT-4000) was used to evaluate the adhesion strength of the films. The measurement was performed at 5 mm min^{-1} and a load increasing rate of 30 N min^{-1}.

2.3 Electrochemical tests

The electrochemical measurements were conducted using an Autolab potentiostat (PGSTAT302N) to assess the corrosion behaviors of the samples. The schematic of the electrochemical test setup was shown in Fig. 1a. A classic three-electrode electrochemical system with a saturated calomel as reference electrode, a platinum sheet as the counter electrode and the sample under study (exposed surface area of 0.5 cm^2) as a working electrode was used. The sample was immersed in the corrosive medium for 30 min to establish a steady open circuit potential (OCP) before the measurements. Potentiodynamic polarization test was performed at a constant weep rate of 10 mV s^{-1}. The corrosion potential (E_{corr}) and the corrosion current density (i_{corr}) were obtained based on the Tafel extrapolation method.[16] The porosity of the film was estimated using an empirical equation.[9,11,25]

$$\text{Porosity} = \frac{R_{p(substrate)}}{R_{p(film)}} \times 10^{-\Delta E_{corr}/\beta_a} \quad (1)$$

where $R_{p(substrate)}$ stands for the polarization resistance of the substrate and $R_{p(film)}$ is the measured polarization resistance of the films. ΔE_{corr} is the potential difference between the corrosion potentials of the film and bare substrate, and β_a is the anodic Tafel slope for the substrate.

Long-term electrochemical impedance spectroscopy (EIS) tests were carried out at the open circuit potential over a frequency range of 100 kHz to 10 mHz, with applied 10 mV sinusoidal perturbations. ZView2 software was used for analyzing the EIS results.

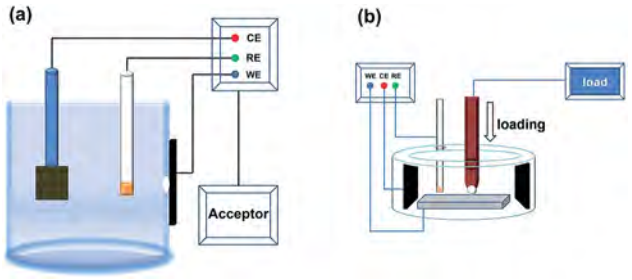

Fig. 1 The schematics of the (a) electrochemical and (b) tribocorrosion test setups.

2.4 Tribocorrosion tests

The tribocorrosion performance of the samples was studied in NaCl solution by using a ball-on-disk tribometer connected with a three electrode electrochemical cell (MFT-EC4000), which was illustrated in Fig. 1b. For the working electrode (WE), the reference electrode (RE) and the counter electrode (CE), the

Table 1 The detailed parameters for depositing the multilayer DLC film and single layer DLC film

Samples	Layers	Ar (sccm)	SiH_4 (sccm)	C_2H_2 (sccm)	Time (min)	Voltage (kV)
Multilayer DLC film	Si_x-DLC	100	50	150	15	−0.8
	Si_y-DLC	100	50	50	10	
Single layer DLC film	Top DLC layer	100	0	150	20	
	DLC layer	100	0	150	120	

samples, a saturated Ag/AgCl and a pure graphite were used, respectively. Tribocorrosion test was carried out under a normal load of 5 N, sliding frequency of 0.15 Hz and stroke length of 5 mm. An alumina ball (Al_2O_3, 6 mm in diameter) was employed as the counterpart due to its chemical inertness under aggressive environments.[26] During the tribocorrosion test, the variation of OCP and the friction coefficient of the samples were studied. The morphology and depth profile of the wear track were analyzed by optical microscopy and surface profilometer (D-100, KLΛ, Tencor), respectively.

3. Results and discussion

3.1 The characterization of the samples

Fig. 2 shows the cross-section microstructure of the films and the depth profiles of the elements. The thickness of the multilayer DLC film and single layer DLC film is approximately 8.0 μm and 3.1 μm, respectively (Fig. 2a and c). EDS line scan result of the single layer DLC film indicates that the film is only composed of carbon (Fig. 2b). AES depth profile of the multilayer DLC film is presented in Fig. 2d, in which a cyclical bilayer composed of low-Si-doped layer (Si_x-DLC) and high-Si-doped layer (Si_y-DLC) can be recognized. This result verifies the multilayer structure of Si_x-DLC/Si_y-DLC observed by SEM. However, it can be observed from Fig. 2 that the single layer DLC film is much thinner than the multilayer DLC film. The main reason is that when DLC films are deposited on the steel substrates, high intrinsic stress and a mismatch in the chemical bonding between the film and substrate often cause for poor adhesion, limiting the film thickness to a range between 1 and 3 μm.[18,27] For multilayer carbon film, the tensile stress and compressive stress in the film can reach equilibrium by growing films a multilayer architecture, thus leading to good adhesion between the film and substrate and the increase in film thickness.

Fig. 3a and c display the SEM surface morphologies of the DLC films. In case of the single layer DLC film, some droplets are produced during the deposition process and the surface is very coarse (Fig. 3a). However, it is evident that the surface becomes smoother and the droplets on the surface decrease dramatically for the multilayer DLC film (Fig. 3c). Meanwhile, AFM is employed to measure the surface roughness of the DLC films. The surface roughness of the single layer DLC film and multilayer DLC film is 6.54 nm and 3.84 nm, respectively (Fig. 3b and d). This clearly indicates that the incorporation of Si can effectively decrease the surface flaws.[26]

Fig. 4a shows the XRD patterns of the samples, which reveals that all diffraction peaks of the DLC films come from the substrate, without the characteristic peaks of carbon compounds.[28] TEM image of the cross-section of the multilayer DLC film displays a periodic structure and distinct multilayer interface (Fig. 4b). The relative dark layers represent the Si_x-DLC layers while the bright ones are the Si_y-DLC layers. More detailed information of two different alternative layers is obtained by HRTEM investigation, as shown in Fig. 4c. The diffuse cloudy FFT patterns of the Si_x-DLC and Si_y-DLC layers indicate the absence of crystalline phase, which confirms that the DLC film is amorphous.[28–30]

Fig. 5 shows the curve-fitted C 1s XPS of the DLC films. Three contributions can be taken into account for C 1s peaks. One from the carbon atoms in the sp^3 boned carbon and the other from the carbon atoms in the sp^2 configuration.[31] The third

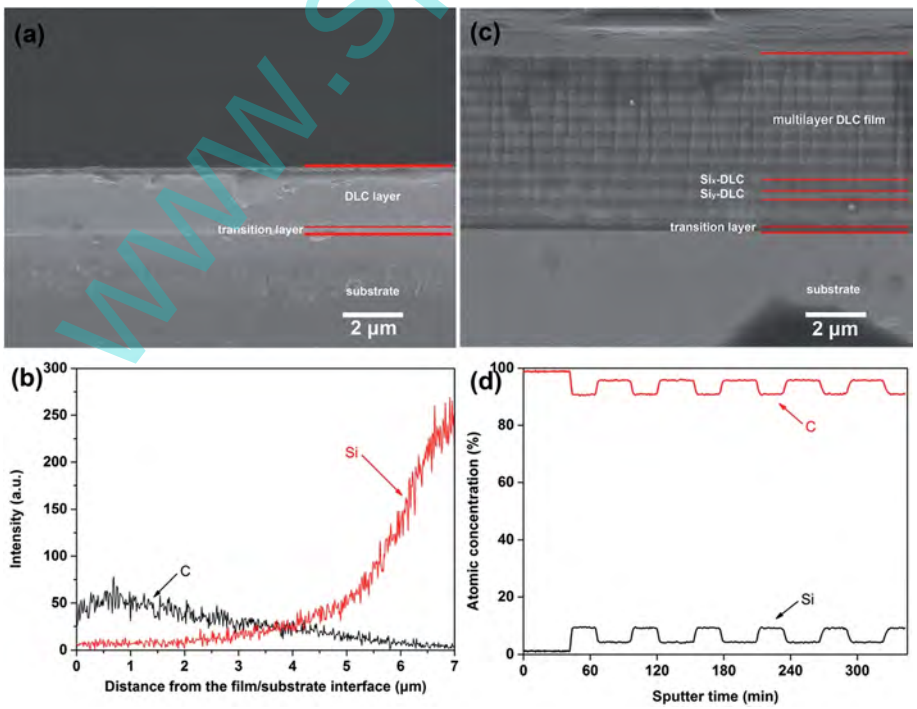

Fig. 2 The cross-section microstructure and the depth profiles of element for the (a and b) single layer DLC film and (c and d) multilayer DLC film.

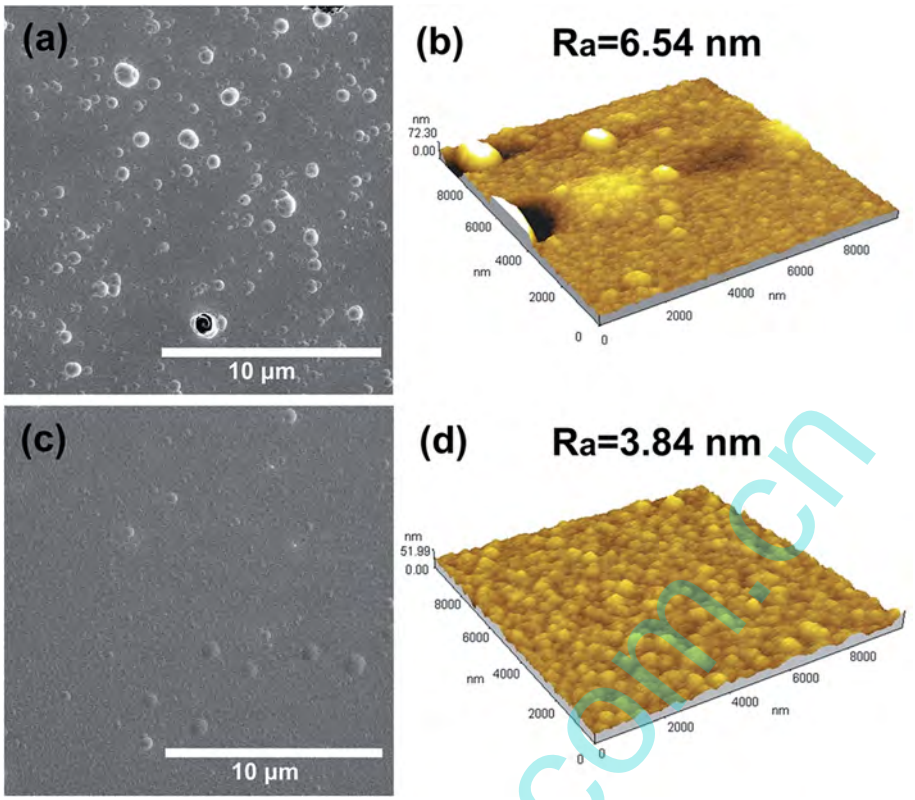

Fig. 3 The SEM and AFM surface morphologies of the (a and b) single layer DLC film and the (c and d) multilayer DLC film.

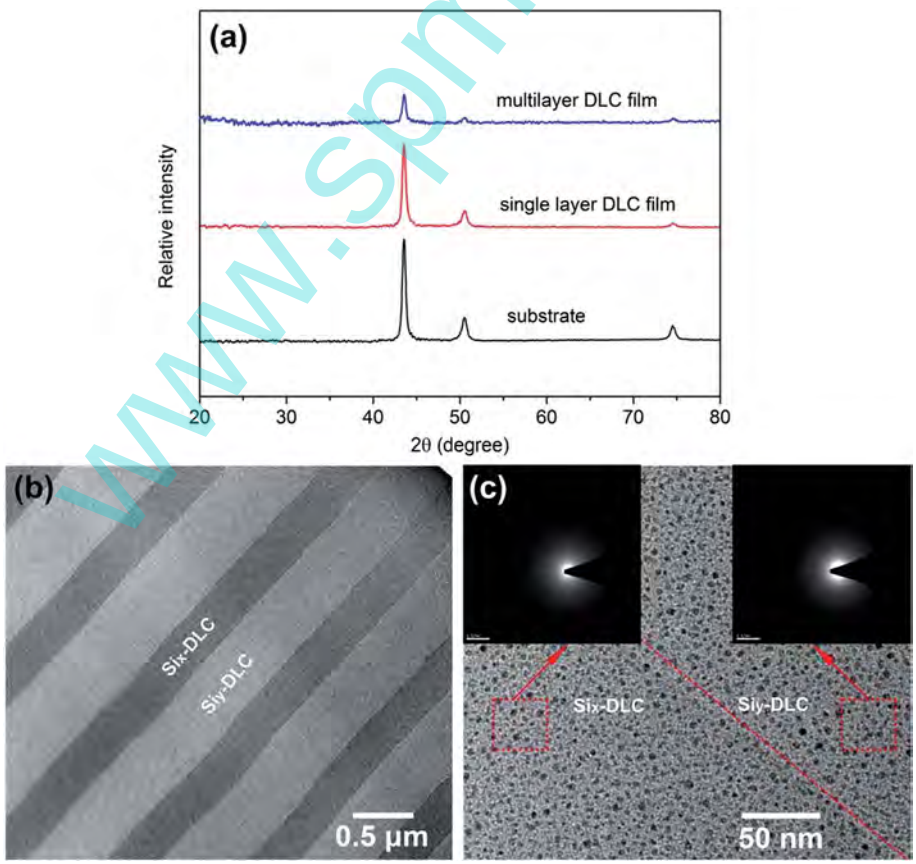

Fig. 4 (a) XRD patterns of the samples, (b and c) the TEM and HRTEM images of Si_x-DLC and Si_y-DLC layers.

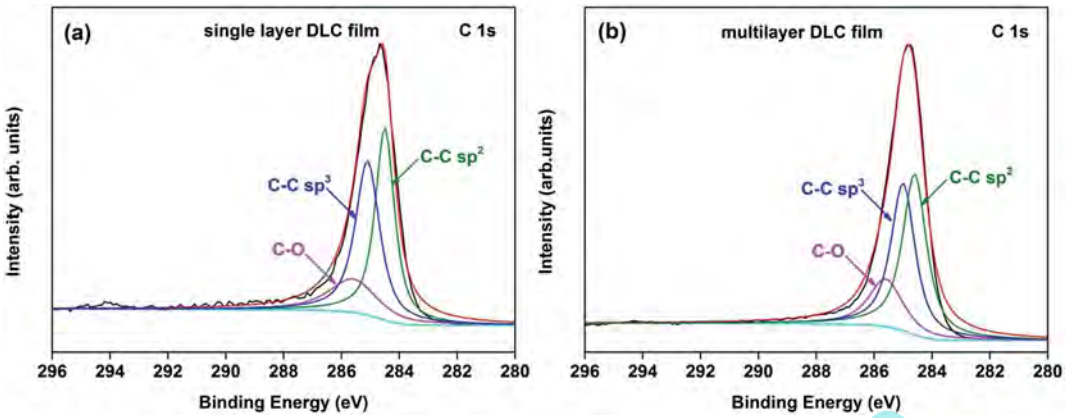

Fig. 5 Deconvoluted C 1s X-ray photoelectron spectra of the DLC films.

peak can be recognized as C–O bonds, which are derived from the surface contamination. The content of "diamond" sp^3 carbon atom has an effect on the corrosion resistance of films according to the reported references,[32,33] and it can be determined from the corresponding peak area.[31,34] The results are summarized in Table 2. It is clearly observed that the sp^3 fraction in two kinds of films has no significant difference.

Fig. 6 presents the scratch tracks of the DLC films with a length of 5 mm and a progressive load from 1 to 30 N. Regarding the scratch track of the single layer DLC film (Fig. 6a), the delamination is observed already at the initial test, which indicates the poor adhesion strength between the film and substrate. In contrast, the multilayer DLC film presents different behavior (Fig. 6b). The white arrow indicates the starting point of the scratch. It is observed that the multilayer DLC film does not present cracking at the beginning of the test, which indicates the highly elastic behavior of the film. It is believed that the film failure is postponed due to the incorporation of Si and alternate layers in the multilayer DLC film which can reduce the residual stress and enhance the adhesion strength between the film and substrate, leading to increased fatigue strength of the film.[25,35]

Table 2 Results of the deconvolution of C 1s XPS peaks

Samples	FWHM sp^3 peak [eV]	FWHM sp^2 peak [eV]	sp^3 content [%]
Single layer DLC film	1.0	1.1	50
Multilayer DLC film	1.0	1.1	48

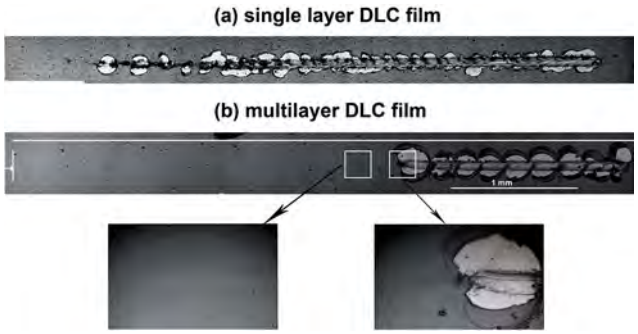

Fig. 6 Scratch tracks of the DLC films.

3.2 Electrochemical evaluation

Fig. 7 shows the potentiodynamic polarization curves of the samples in 3.5 wt% NaCl solution. The corrosion potential (E_{corr}) and the corrosion current density (i_{corr}) are listed in Table 3. Generally, the corrosion resistance of the samples depends on the corrosion current density.[6] The lower the corrosion current density is, the higher the corrosion resistance is. It is clear that the multilayer DLC film holds the lowest corrosion current density, and a wide "passive-like" region with a low anodic current density can be observed. These confirm the high corrosion resistance of the multilayer DLC film in 3.5 wt% NaCl solution. After the potentiodynamic polarization test, the surface morphology and corrosion features of the samples are checked by SEM and the corresponding micrographs are shown in Fig. 8. Pitting corrosion has occurred at the substrate surface

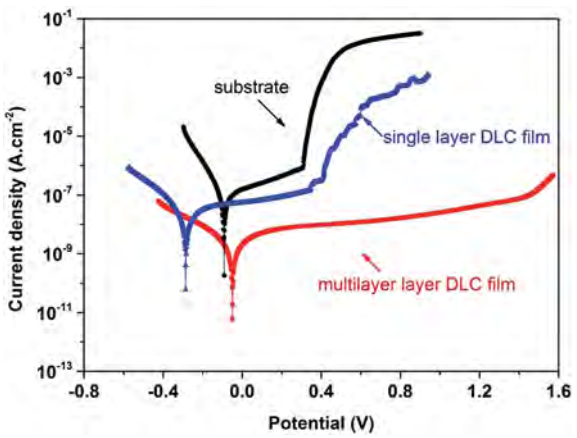

Fig. 7 The potentiodynamic polarization curves of the samples in 3.5 wt% NaCl solution.

Table 3 The corrosion potential (E_{corr}) and corrosion current density (i_{corr}) obtained from potentiodynamic polarization curves

Samples	E_{corr} (V)	i_{corr} (A cm^{-2})
Substrate	−0.093	1.08×10^{-7}
Single layer DLC film	−0.29	1.10×10^{-7}
Multilayer DLC film	−0.049	8.94×10^{-9}

(Fig. 8b) and some pores also present in the surface of the single layer DLC film (Fig. 8d), whereas no significant damage is observed in the surface of multilayer DLC film (Fig. 8f). This clearly indicates that the multilayer DLC film has excellent corrosion resistance.

Fig. 9 presents the EIS plots of the samples obtained after 2, 5, 10, 20, 35 and 50 h of exposure. For the substrate, the total impedance values of the system increase systematically from 3×10^5 to 2×10^6 Ω cm^2 within 50 h of immersion. The phase angle plots of the substrate reveal a broadened time constant, which is attributed to the presence of the passive film at the substrate surface.

As for the coated substrates, totally different corrosive behaviors are observed within 50 h immersion (Fig. 9c–f). In case of the single layer DLC film, the total impedance values have no obvious change (4×10^7–6×10^7 Ω cm^2) during 50 h of immersion. At 2–35 h immersion times, two time constants are observed. The first time constant in the high and intermediate frequencies is characteristic for the capacitive response of the single layer DLC film. The low-frequency time constant appears to be a result of the diffusion process in the single layer DLC film through the micro- and nanopores. However, after 50 h of immersion, a new capacitive response emerges. This change is mainly ascribed to the evolution of corrosion product layer during the immersion, indicating that the electrolyte has reached to the substrate. In regard to the multilayer DLC film, there also is no significant difference between the impedance values (5.4×10^7 Ω cm^2) during 50 h of immersion. And three incomplete time constants with different relaxation time occur during 50 h of immersion. The one at high and middle frequencies can be ascribed to the capacitive response of the multilayer DLC film, another at 0.1–1 Hz is related to the formation of a double layer of charge at the multilayer DLC film–electrolyte interface, while at the low frequencies (0.01–0.1 Hz) the impedance behavior comes from the contribution of a diffusion process.

To better understand the corrosion behaviors of the samples in NaCl electrolyte, EIS results are fitted using equivalent circuits shown in Fig. 10. The equivalent circuits consist of the following elements: the solution resistance R_s; the capacitance of the passive film formed at the substrate surface CPE_1; the resistance of the passive film R_1; R_f stands for the pore resistance of the films paralleled with constant phase element CPE_f; the double layer capacitance is represented as CPE_{dl1} due to the formation of a double layer of charge at the substrate–electrolyte interface, and the corresponding polarization resistance is R_{p1}; the double layer capacitance at DLC film–electrolyte interface C_{dl2}, the corresponding polarization resistance R_{p2}. W_0 is the Warburg impedance, which is attributed to the diffusion process of the corrosive medium in the film or from solution to the electrode surface.[36]

Tables 4–6 summarize the corresponding circuit parameters obtained from fitting process. In case of the substrate (Table 4), the increased resistances (R_1) and decreased capacitances (CPE_1) are mainly due to the build-up of passive film, which serves as a protective barrier against the permeation of corrosive medium to substrate.

Table 5 gives the fitting results of the single layer DLC film. At 2–35 h immersion times, the values of R_f are relatively steady while the values of W_0 show a declining trend. At this stage, the corrosion process is probably controlled by the diffusion

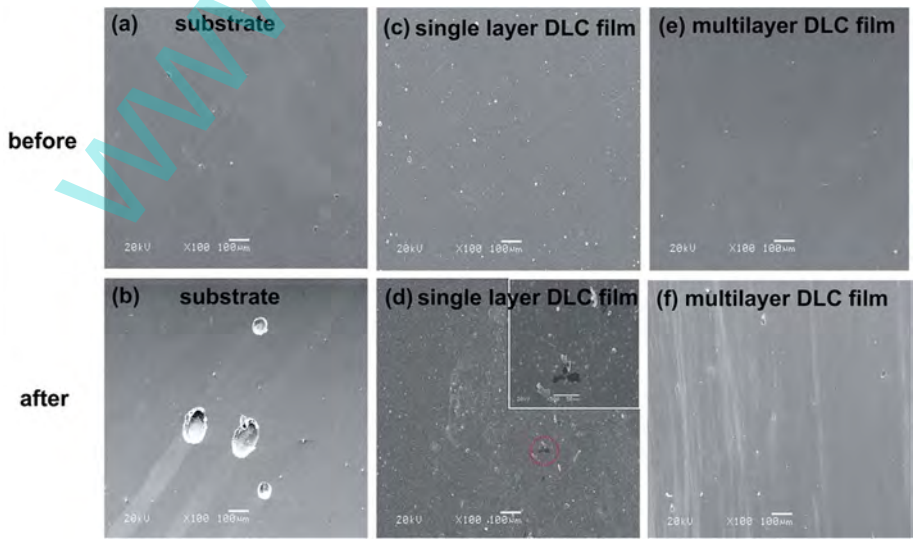

Fig. 8 The SEM surface morphology before and after potentiodynamic polarization scans on the (a and b) substrate, (c and d) single layer DLC film, and (e and f) multilayer DLC film.

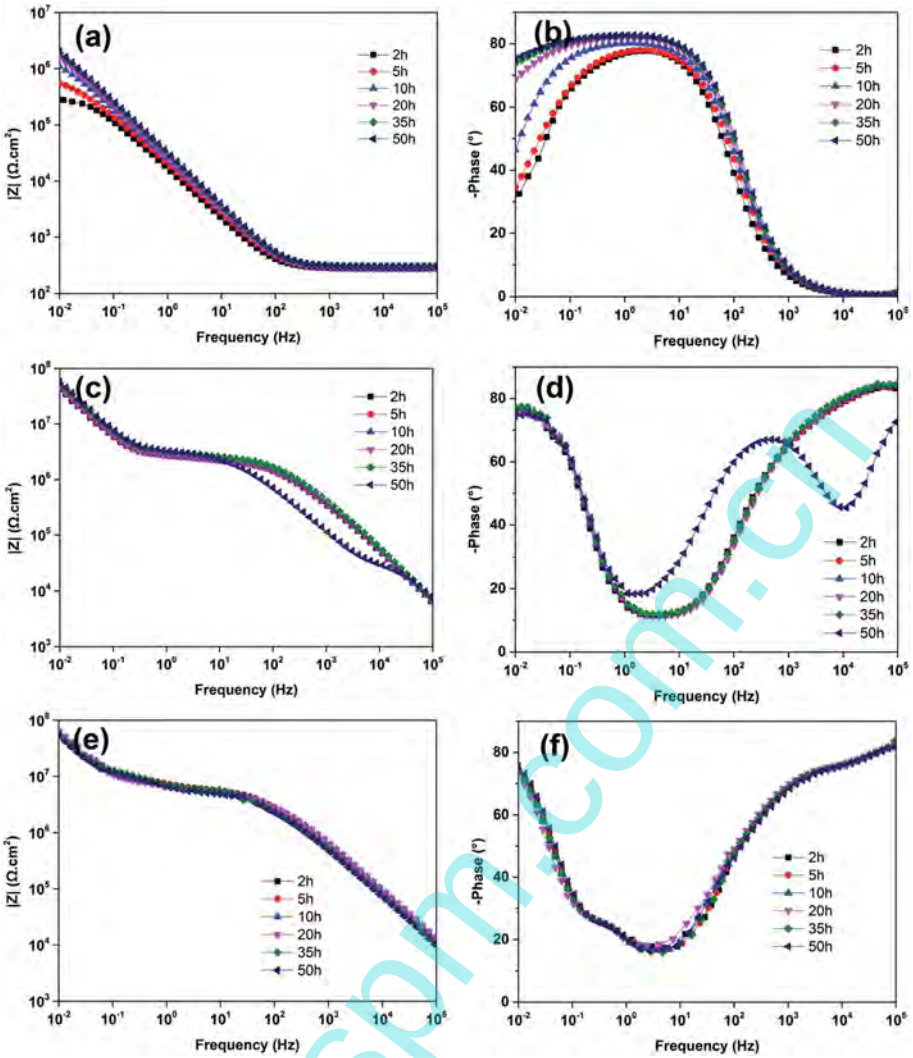

Fig. 9 EIS bode plots of the samples obtained after 50 h electrochemical test in 3.5 wt% NaCl solution, (a and b) substrate, (c and d) single layer DLC film, (e and f) multilayer DLC film.

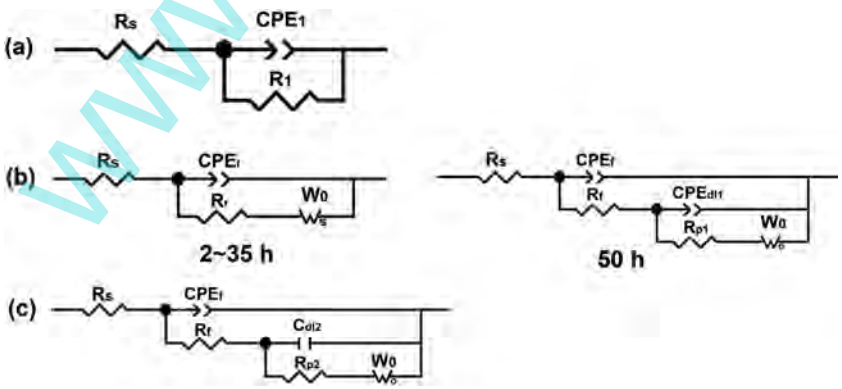

Fig. 10 Equivalent circuits employed to fit EIS results. (a) Substrate, (b) single layer DLC film, (c) multilayer DLC film.

process. The main reason is that the carbon layer in the single layer DLC film is chemically inert to NaCl solution and the increase in porosity or pore size makes electrolyte easier to diffuse within the film, thus leading to the decrease of the W_0. After 50 h of immersion, a new capacitive response emerges and the value of R_f decreases abruptly. This indicates that electrolyte has reached to the substrate and the film has started to deteriorate.[37] Combined with the polarization result, we can

Table 4 The fitting results of the EIS plots of the substrate during 50 h of immersion

	CPE_1	n	R_1 (Ω cm^2)
2 h	1.2×10^{-5}	0.89	3.9×10^5
5 h	1.0×10^{-5}	0.89	7.0×10^5
10 h	8.1×10^{-6}	0.91	1.8×10^6
20 h	7.1×10^{-6}	0.92	5.5×10^6
35 h	6.1×10^{-6}	0.92	1.0×10^7
50 h	5.8×10^{-6}	0.93	1.2×10^7

conclude that the single layer DLC film is not effective to prevent the substrate from long-term corrosion attack.

In case of the multilayer DLC film (Table 6), the values of R_f have no obvious change during 50 h of immersion. However, it can be seen from Table 6 that the polarization or charge transfer resistance (R_{p2}) increases during the first 20 h of immersion and then decrease with the increase of immersion time. Similar behavior of the Warburg impedance with exposure time is also observed. We believe that the variation of porosity for the film during the immersion may account for this phenomenon. To confirm our suspicion, the porosity of the multilayer DLC film during 50 h of immersion is summarized in Table 7 according to the empirical eqn (1). Results showed that the porosity of the multilayer DLC film decreased with time at 0.5–30 h immersion times, suggesting that corrosion product (insulting Si oxides) was gradually formed on the film surfaces and blocked the pores within the films.[38,39] As a result, the diffusion of electrolyte or the chloride ions becomes more difficult, evidenced by the increase in Warburg impedance of the multilayer DLC film, thus resulting in the inhibition of corrosion.[16] Therefore, at this stage, the corrosion of the film is mainly controlled by the formation of Si oxides. With the increasing of immersion time, porosity increases and Warburg impedance decreases,

Table 7 The variation in porosity of the multilayer DLC film during 50 h of immersion

	0.5 h	2 h	5 h	10 h	20 h	30 h	40 h	50 h
Porosity (10^{-2})	0.51	0.58	0.44	0.31	0.33	0.30	0.40	0.36

indicating that the ion conductive path through the pores is greatly enlarged and the diffusion of electrolyte or the chloride ions becomes easier.[40] Therefore, the corrosion process is probably controlled by the diffusion of electrolyte at this stage.

Fig. 11 presents the variation in Si 2p XPS intensity of the multilayer DLC film as deposited and after long-term EIS tests. Only the variation of Si is analyzed, because the carbon and oxygen signals in XPS may originate from contamination of the sample surface and they are usually not reliable. Result shows that the intensity of Si 2p peak increases dramatically after long-term EIS test, which is possibly caused by the etching of the top DLC layer in the solution. The peaks for Si 2p can be resolved into two contributions: the peak at 102.8 eV is consistent with the Si–C bonds, and the peak at around 100.3 eV mostly rises from Si bonded to O.[18] The intensity of Si–O bond increases obviously after 50 h of immersion, suggesting the formation of the insulting Si oxides, which is favorable to reduce the porosity and improve films' anticorrosion abilities.[16,34]

Meanwhile, SEM morphologies for corroded surfaces after long-term immersion were also checked. As shown in Fig. 12a, some big and shallow pits distribute around the droplets for the single layer DLC film, which indicates that the corrosion initiates from the droplets. In case of the multilayer DLC film, the images display no obvious damage of surface after 20 h and 50 h of immersion, which confirms that the multilayer DLC film has better corrosion performance in long-term corrosion attack.

It is worth noting that although the difference in the pore resistance of the single layer DLC film and the multilayer DLC

Table 5 The fitting results of the EIS plots of the single layer DLC film during 50 h of immersion

	CPE_f	n	R_f (Ω cm^2)	CPE_{dl1}	n	R_{p1} (Ω cm^2)	W_0 (Ω cm^2)
2 h	1.1×10^{-9}	0.89	1.8×10^6	—	—	—	2.4×10^6
5 h	1.0×10^{-9}	0.89	1.8×10^6	—	—	—	2.3×10^6
10 h	9.6×10^{-10}	0.90	1.9×10^6	—	—	—	2.2×10^6
20 h	8.5×10^{-10}	0.91	1.9×10^6	—	—	—	1.9×10^6
35 h	8.0×10^{-10}	0.91	2.2×10^6	—	—	—	2.5×10^6
50 h	2.9×10^{-10}	0.97	3.2×10^4	5.0×10^{-9}	0.84	2.5×10^6	2.2×10^6

Table 6 The fitting results of the EIS plots of the multilayer DLC film during 50 h of immersion

	CPE_f	n	R_f (Ω cm^2)	C_{dl2}	R_{p2} (Ω cm^2)	W_0 (Ω cm^2)
2 h	9.1×10^{-10}	0.87	2.5×10^6	5.5×10^{-10}	1.8×10^6	1.7×10^7
5 h	9.0×10^{-10}	0.87	2.5×10^6	5.2×10^{-10}	1.9×10^6	1.7×10^7
10 h	8.5×10^{-10}	0.88	2.4×10^6	4.6×10^{-10}	2.3×10^6	1.8×10^7
20 h	8.2×10^{-10}	0.88	2.5×10^6	4.0×10^{-10}	2.7×10^6	2.2×10^7
35 h	9.9×10^{-10}	0.87	3.2×10^6	6.8×10^{-10}	1.7×10^6	1.8×10^7
50 h	8.9×10^{-10}	0.87	2.2×10^6	2.1×10^{-10}	2.1×10^6	1.5×10^7

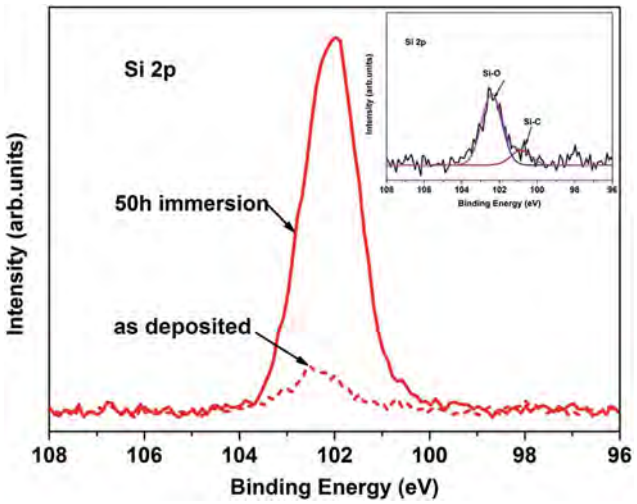

Fig. 11 Si 2p XPS of the multilayer DLC film as deposited and after the long-term EIS tests.

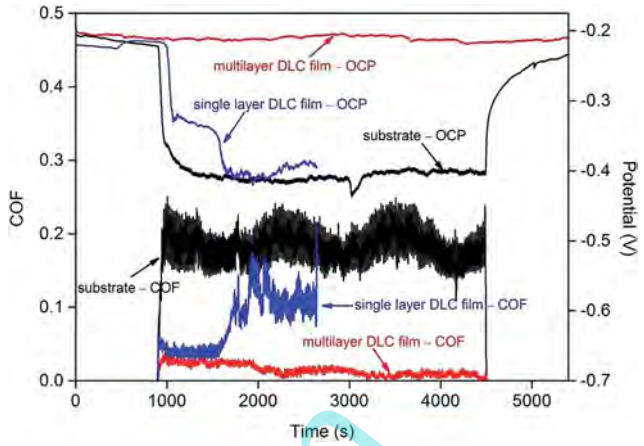

Fig. 13 Variation in OCP and friction coefficient curves during the tribocorrosion test in 3.5 wt% NaCl solution.

film is not significant during 50 h of immersion, the multilayer DLC film shows much larger Warburg impedance value than that of the single layer DLC film as can be seen from Tables 5 and 6. This is mainly because the multilayer structure enhances barrier effect and prolongs the diffused paths of corrosive medium.[4,6,41] In addition, the formation of Si oxides can impede the degradation of the film in some extent,[16,38] leading to the excellent long-term corrosion resistance of the multilayer DLC film. As we know, other processes besides corrosion act simultaneously in a real situation.[39] Thus, wear-corrosion test should be performed to adequately evaluate the properties of the samples.

3.3 Tribocorrosion evaluation

The OCP and friction coefficient curves of the samples during the tribocorrosion test are shown in Fig. 13. For the substrate, OCP stabilized after 900 s, indicating a stable electrochemical condition on the surface.[42] Rapid negative shift of the OCP was observed when the load was applied. This was mainly attributed to the damage of passive film caused by sliding contact and subsequent exposure of activated surface in NaCl solution.[2,3] When the sliding ceased, the OCP first steeply increased and then progressively reached a steady state value, which was proclaimed as a recovery of the damaged passive film.[2,3] The fluctuation of friction coefficient during sliding was obvious, and the average friction coefficient was about 0.2. In the case of the single layer DLC film, a sudden drop of the OCP value was observed at the initial sliding, which suggested that the film was locally removed. The OCP value was approximately −0.3 V. After 600 s sliding, there was a negative shift for OCP again. This indicated that the single layer DLC film had been worn out and the substrate at local position was exposed in the NaCl solution. The variation of friction coefficient for the single layer DLC film was consistent with that of the OCP. The possible reason is the poor adhesion strength between the single layer DLC film and substrate. Whereas rubbing produced only a very slight effect on

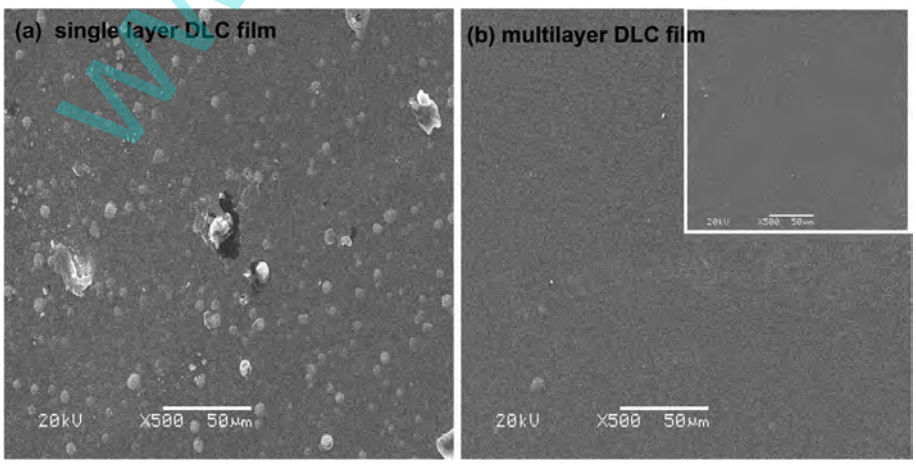

Fig. 12 SEM morphologies for corroded surfaces of the single layer DLC film and the multilayer DLC film after long-term immersion (the inset shows a SEM image after 20 h of immersion).

the OCP for the multilayer DLC film, which remained almost constant throughout the entire test. During the first few cycles, the average friction coefficient was about 0.025. Subsequently, it progressively decreased to reach 0.010.

Fig. 14 shows the optical microscopy images and profile of wear tracks of the samples. It is clearly seen that numerous ploughed grooves appear in the wear track of substrate and the single layer DLC film delaminates from the substrate, whereas the surface of multilayer DLC film has no obvious damage. Moreover, the substrate and single layer DLC film exhibit deep grove with depths about 1500 nm and 2900 nm, respectively, while the multilayer DLC film displays shallow groves with depth bellow 150 nm. The wear rate of the samples is listed in Table 8. The wear rate of the multilayer DLC film is the lowest among the tested samples in corrosive medium. This accounts for why the OCP of the multilayer DLC film remains almost constant during the tribocorrosion test. Wu *et al.* found that tribochemical reaction of the Si-DLC coating occurred in water resulting in the formation of $SiO_x(OH)_y$ gel, which could reduce the friction in a water environment.[43] And in our previous work, the multilayer DLC film exhibited superior wear and corrosion

Table 8 The wear rate of the samples

Samples	substrate	single layer DLC film	multilayer DLC film
Wear rate (10^{-6} mm^3 N^{-1} m^{-1})	30.8	Wear out	1.48

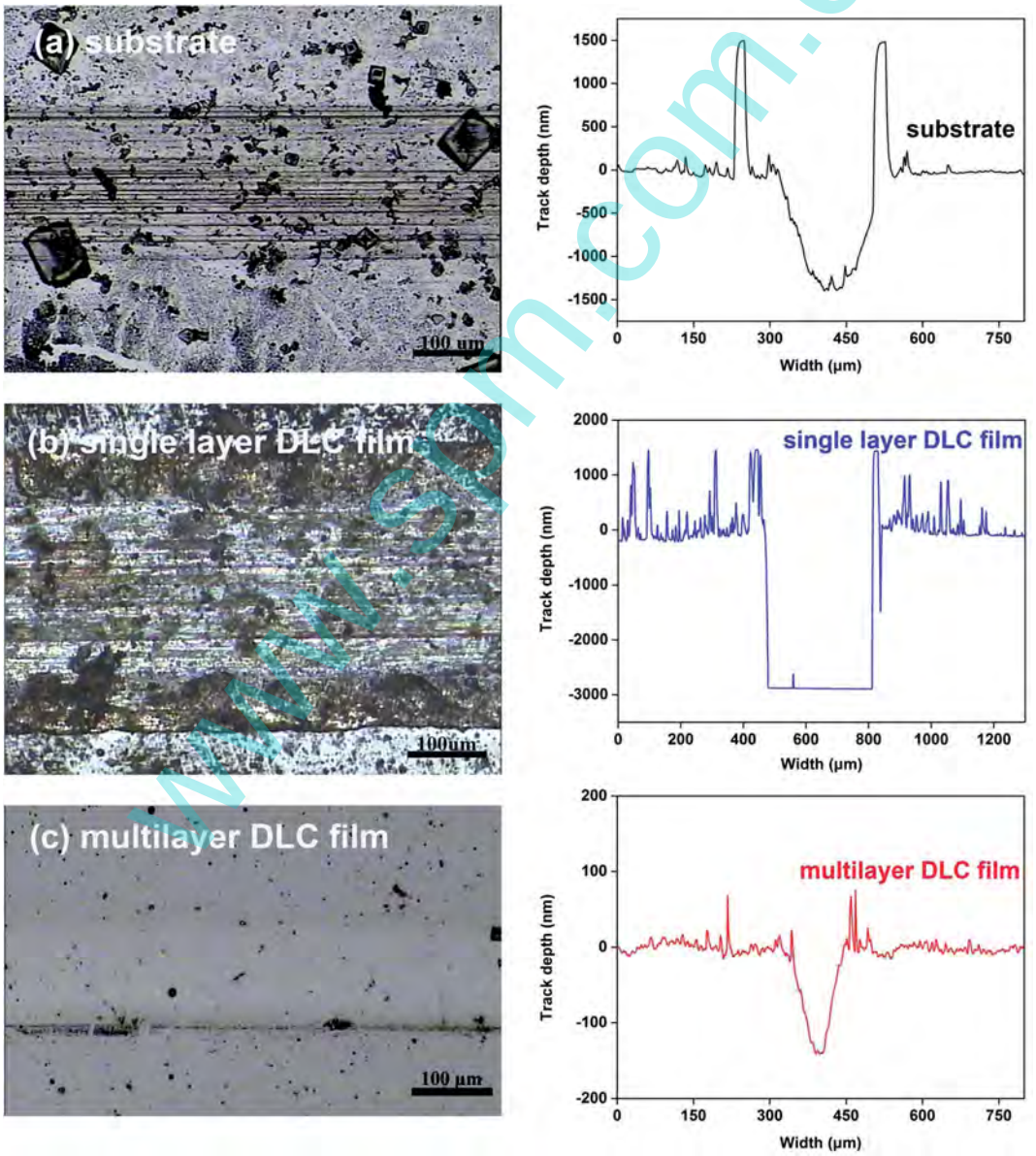

Fig. 14 The optical microscopy images and profiles of wear tracks after the tribocorrosion test in 3.5 wt% NaCl solution (a and b) Substrate, (c and d) single layer DLC film, (e and f) multilayer DLC film.

resistance in HCl solution, we believed that the solid-like film and SiC nanocrystallines were responsible for the excellent wear reduction in HCl solution.[44] Thus, the tribocorrosion performance of the DLC films was assign to the variable mechanisms, we would investigate the detailed tribocorrosion mechanism in our next work.

4. Conclusions

In this study, multilayer DLC films were prepared by the PECVD method. Their corrosion and tribocorrosion properties were systematically investigated in 3.5 wt% NaCl solution. The conclusions can be summarized as follows:

(1) The multilayer DLC film has a lower corrosion current density as comparison with the substrate and single layer DLC film, leading to the excellent corrosion performance. Meanwhile, an extremely stable EIS behavior and high Warburg impedance value of the multilayer DLC film during 50 h of immersion also confirm the superior barrier properties. This can be attributed to the multilayer structure and the formation of Si oxides providing better resistance to diffusion of corrosive solution into the films.

(2) Tribocorrosion resistance of the multilayer DLC film is significantly improved compared to other samples. Moreover, an extremely low wear rate under NaCl conditions is achieved for the multilayer DLC film.

Acknowledgements

The authors gratefully acknowledged financial support provided by the National Key Basic Research Program (No. 2014CB643302) and National Natural Science Foundation of China (Grant No. 51322508). The authors also gratefully acknowledged Prof. Jun Wang for performing electrochemical measurements.

References

1 R. Bayón, R. Nevshupa, C. Zubizarreta, U. R. de Gopegui, J. Barriga and A. Igartua, *Anal. Bioanal. Chem.*, 2010, **396**, 2855–2862.
2 Y. Sun and V. Rana, *Mater. Chem. Phys.*, 2011, **129**, 1138–1147.
3 Y. Zhang, X. Y. Yin, J. Z. Wang and F. Y. Yan, *Corros. Sci.*, 2014, **88**, 423–433.
4 L. A. Dobrzański, K. Lukaszkowicz, D. Pakuła and J. Mikuła, *Arch. Mater. Sci. Eng.*, 2007, **28**, 12–18.
5 G. H. Song, X. P. Yang, G. L. Xiong, Z. Lou and L. J. Chen, *Vacuum*, 2013, **89**, 136–141.
6 C. Liu, A. Leyland, Q. Bi and A. Matthews, *Surf. Coat. Technol.*, 2001, **141**, 164–173.
7 R. Bayón, A. Igartua, X. Fernández, R. Martínez, R. J. Rodríguez, J. A. García, A. de Frutos, M. A. Arenas and J. de Damborenea, *Tribol. Int.*, 2009, **42**, 591–599.
8 J. D. Beard, S. Aleksandrov, C. H. Walker, D. Wolverson, J. M. Mitchelsc and S. N. Gordeev, *RSC Adv.*, 2014, **4**, 26635–26644.
9 H. G. Kim, S. H. Ahn, J. G. Kim, S. J. Park and K. R. Lee, *Diamond Relat. Mater.*, 2005, **14**, 35–41.
10 N. Yamauchi, A. Okamoto, H. Tukahara, K. Demizu, N. Ueda, T. Sone and Y. Hirose, *Surf. Coat. Technol.*, 2003, **174–175**, 465–469.
11 L. Joska and J. Fojt, *Appl. Surf. Sci.*, 2012, **262**, 234–239.
12 D. Bootkul, B. Supsermpol, N. Saenphinit, C. Aramwit and S. Intarasiri, *Appl. Surf. Sci.*, 2014, **310**, 284–292.
13 L. F. Zhang, F. G. Wang, Q. Li, K. X. Gao, B. Zhang and J. Y. Zhang, *RSC Adv.*, 2015, **5**, 9635–9649.
14 J. H. Sui, Z. G. Zhang and W. Cai, *Nucl. Instrum. Methods Phys. Res., Sect. B*, 2009, **267**, 2475–2479.
15 M. Lubwama, K. A. McDonnell, J. B. Kirabira, A. Sebbit, K. Sayers, D. Dowling and B. Corcoran, *Surf. Coat. Technol.*, 2012, **206**, 4585–4593.
16 J. Choi, M. Kawaguchi, T. Kato and M. Ikeyam, *Microsyst. Technol.*, 2007, **13**, 1353–1358.
17 Z. M. Wang, J. Zhang, X. Han, Q. F. Li, Z. L. Wang and R. H. Wei, *Corros. Sci.*, 2014, **86**, 261–267.
18 J. Wang, J. Pu, G. Zhang and L. Wang, *ACS Appl. Mater. Interfaces*, 2013, **5**, 5015–5024.
19 Z. Xu, Y. J. Zheng, F. Jiang, Y. X. Leng, H. Sun and N. Huang, *Appl. Surf. Sci.*, 2013, **264**, 207–212.
20 L. A. Dobrzański, K. Lukaszkowicz, A. Zarychta and L. Cunha, *J. Mater. Process. Technol.*, 2005, **164–165**, 816–821.
21 Y. Uematsu, T. Kakiuchi, T. Teratani, Y. Harada and K. Tokaji, *Surf. Coat. Technol.*, 2011, **205**, 2778–2784.
22 K. Feng, Z. Li, F. Lu, J. Huang, X. Cai and Y. Wu, *J. Power Sources*, 2014, **249**, 299–305.
23 R. Bayón, A. Igartua, X. Fernández, R. Martínez, R. J. Rodríguez, J. A. García, A. de Frutos, M. A. Arenas and J. de Damborenea, *Tribol. Int.*, 2009, **42**, 591–599.
24 T. Takeshita, Y. Kurata and S. J. Hasegawa, *Appl. Phys.*, 1992, **71**, 5395.
25 T. M. Manhabosco, A. P. M. Barboza, R. J. C. Batista, B. R. A. Neves and I. L. Müller, *Diamond Relat. Mater.*, 2013, **31**, 58–64.
26 H. G. Kim, S. H. Ahn, J. G. Kim, S. J. Park and K. R. Lee, *Thin Solid Films*, 2005, **482**, 299–304.
27 K. W. Chen and J. F. Lin, *Thin Solid Films*, 2009, **517**, 4916–4920.
28 S. S. Hadinata, M. T. Lee, S. J. Pan, W. T. Tsai, C. Y. Tai and C. F. Shih, *Thin Solid Films*, 2013, **529**, 412–416.
29 E. D. Rejowski, M. C. L. de Oliveira, R. A. Antunes and M. F. Pillis, *J. Mater. Eng. Perform.*, 2014, **23**, 3926–3933.
30 W. Zhu, C. Y. Nie, C. H. Ran, Y. D. Jin and Y. Zhao, *Adv. Mater. Res.*, 2013, **750**, 1977–1981.
31 X. Yan, T. Xu, G. Chen, S. Yang and H. Liu, *Appl. Surf. Sci.*, 2004, **236**, 328–335.
32 R. D. Mansano, M. Massi, A. P. Mousinho, L. S. Zambom and L. G. Neto, *Diamond Relat. Mater.*, 2003, **12**, 749–752.
33 J. H. Sui, Z. Y. Gao, W. Cai and Z. G. Zhang, *Mater. Sci. Eng., A*, 2007, **454**, 472–476.
34 T. Kocourek, M. Jelinek, V. Vorlíček, J. Zemek, T. Janča, V. Žížková and C. Popov, *Appl. Phys.*, 2008, **93**, 627–632.
35 J. M. Lackner, W. Waldhauser, B. Major, L. Major and M. Kot, *Thin Solid Films*, 2013, **534**, 417–425.

36 F. Rosalbino, E. Angelini, D. Macciò, A. Saccone and S. Delfino, *Electrochim. Acta*, 2009, **54**, 1204–1209.
37 C. N. Cao and J. Q. Zhang, *Science*, Beijing, 2002, p. 21.
38 P. Papakonstantinou, J. F. Zhao, A. Richardot, E. T. McAdams and J. A. McLaughlin, *Diamond Relat. Mater.*, 2002, **11**, 1124–1129.
39 T. M. Manhabosco, L. A. M. Martins, S. M. Tamborim, M. Ilha, M. Q. Vieira, F. C. R. Guma and I. L. Müller, *Corros. Sci.*, 2013, **66**, 169–176.
40 D. D. Macdonald, *Electrochim. Acta*, 2006, **51**, 1376–1388.
41 D. H. Chen, N. Jin, W. W. Chen, L. Wang, S. Q. Zhao and D. W. Luo, *Surf. Coat. Technol.*, 2014, **254**, 440–446.
42 M. Azzi, M. Paquette, J. A. Szpunar, J. E. Klemberg-Sapieha and L. Martinu, *Wear*, 2009, **267**, 860–866.
43 X. Wu, M. Suzuki, T. Ohana and A. Tanaka, *Diamond Relat. Mater.*, 2008, **17**, 7–12.
44 R. Zhang and L. Wang, *Surf. Coat. Technol.*, 2015, **276**, 626–635.